Supporting information

Interface-modified $NiMgO_x$ Layers with Dibenzocarbazole Molecules for High-Efficiency Perovskite Light-Emitting Diodes

*Hyungdoh Lee, Jun-Seo Lee, Seungmin Shin, Wonjeong Yu, In Hye Kwak, Hyung Joong Yun, Seungbum Hong, and Himchan Cho**

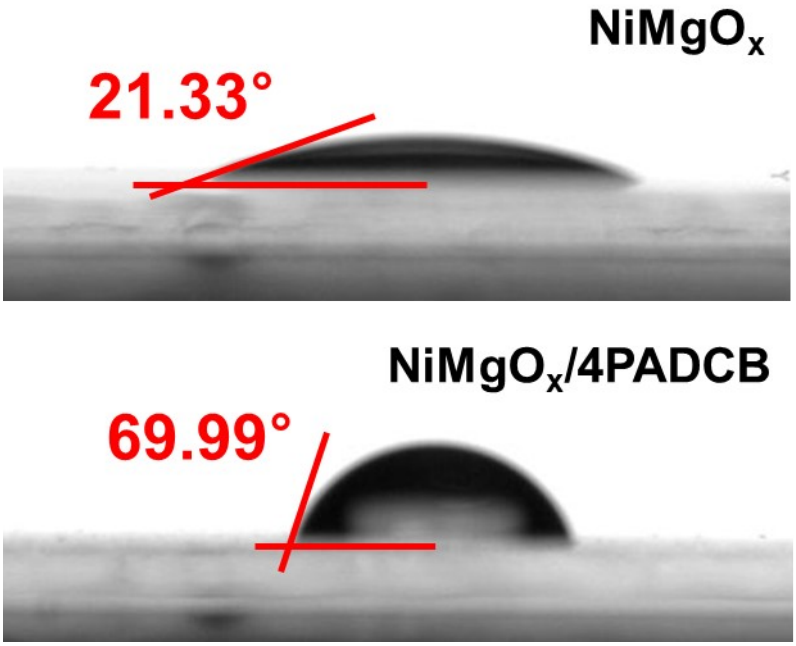

Figure S1. Water contact angle of $NiMgO_x$ surface with and without 4PADCB interlayers.

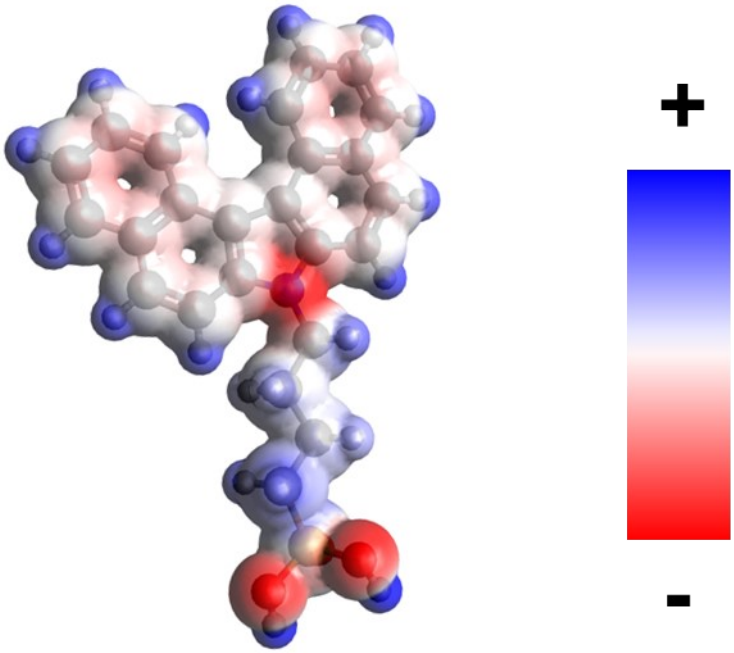

Figure S2. Electrostatic potential (ESP) mapping image of 4PADCB molecule.

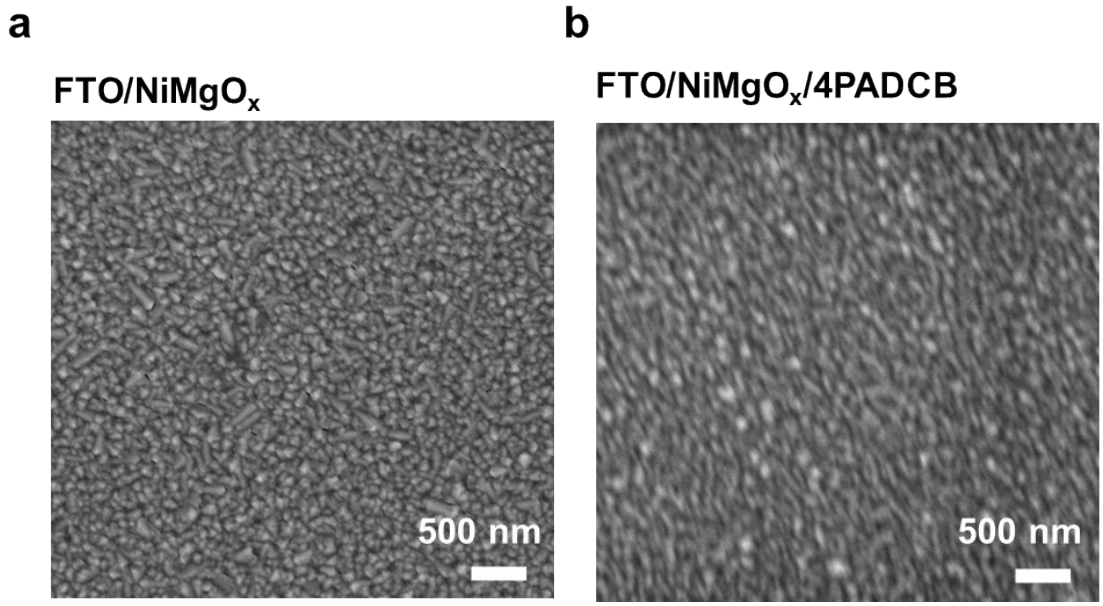

Figure S3. Scanning electron microscopy (SEM) image of (a) FTO/NiMgO$_x$ and (b) FTO/NiMgO$_x$/4PADCB surface.

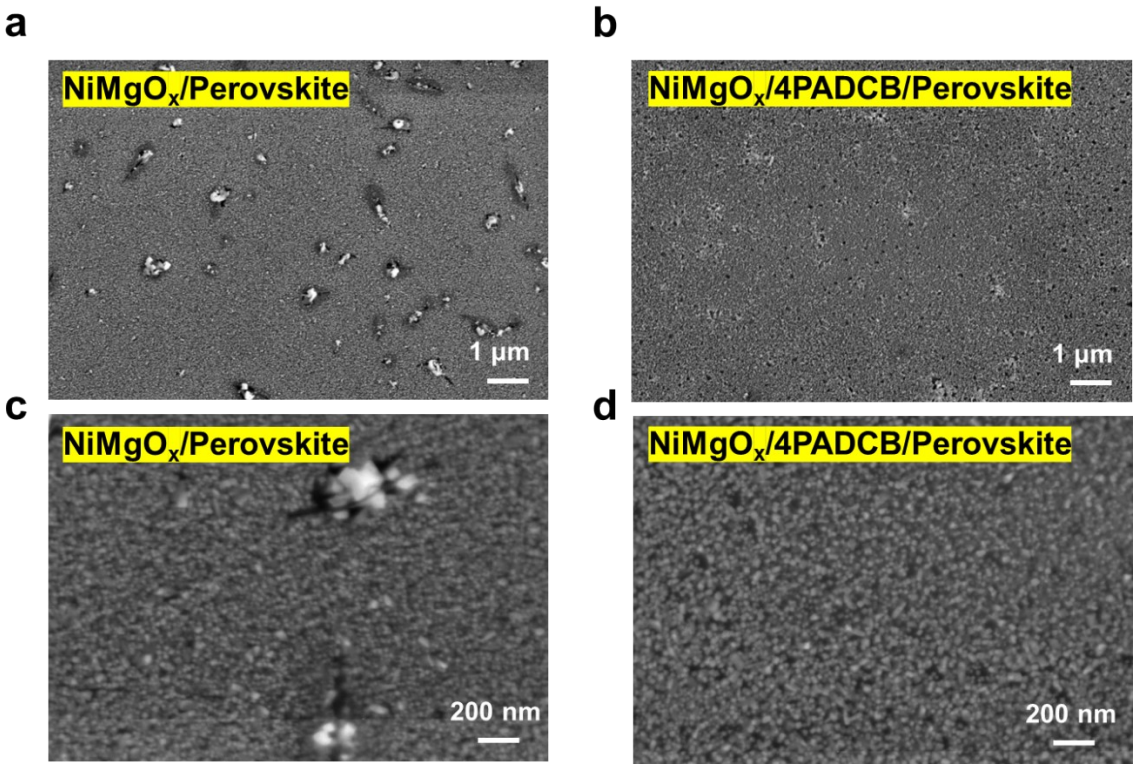

Figure S4. Surface morphology analysis of perovskite films deposited on different underlying layers. a) Scanning Electron Microscopy (SEM) image of the perovskite film surface on the pristine $NiMgO_x$ substrate and b) on the $NiMgO_x$/4PADCB surfaces. c) High-magnification SEM image of the perovskite surface on $NiMgO_x$ and d) on $NiMgO_x$/4PADCB.

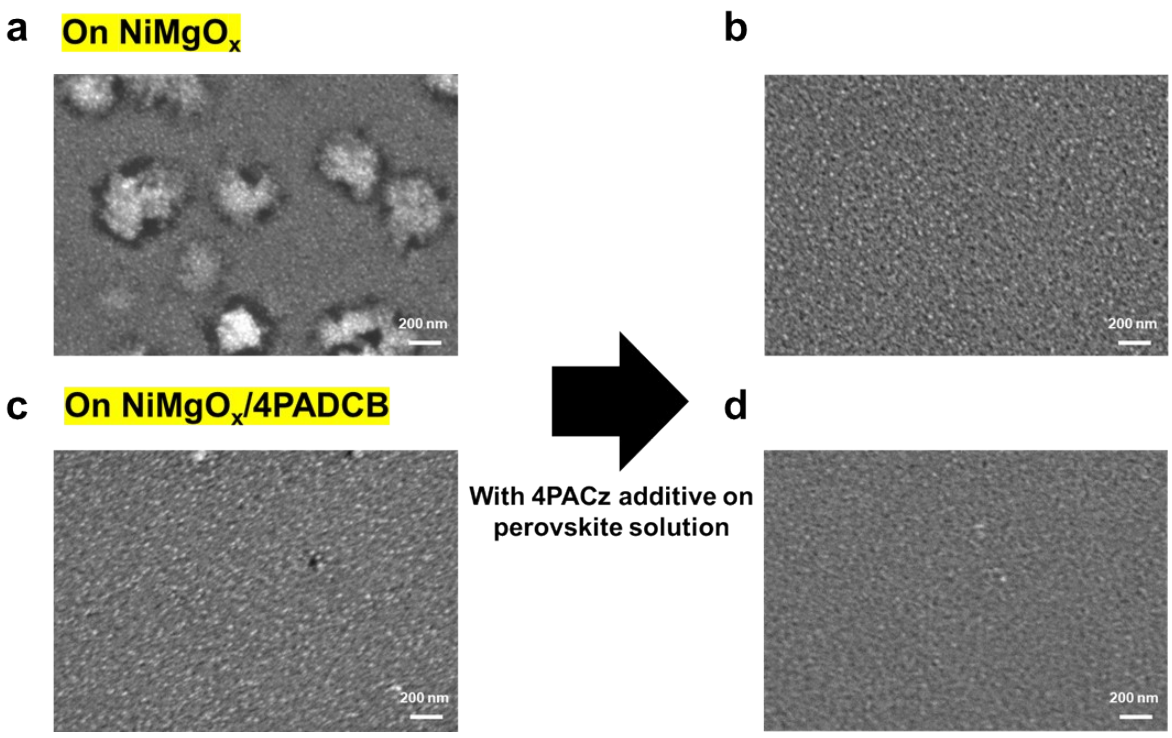

Figure S5. SEM analysis of perovskite film morphology showing films fabricated a,c) without and b,d) with the 4PACz additive in perovskite precursor solution, comparing deposition on a,b) the pristine $NiMgO_x$ and c,d) the $NiMgO_x$/4PADCB surfaces.

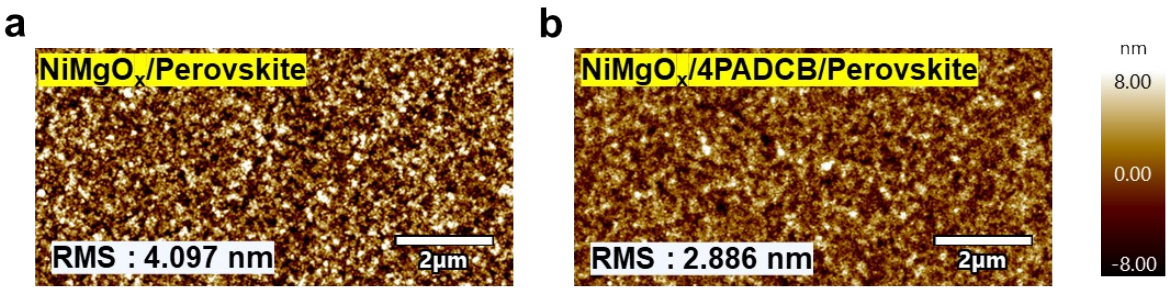

Figure S6. Surface topography analysis of perovskite films via Atomic Force Microscopy (AFM). a) AFM image and corresponding surface roughness data for the perovskite film deposited on the pristine $NiMgO_x$ layer and b) on the $NiMgO_x$/4PADCB interface.

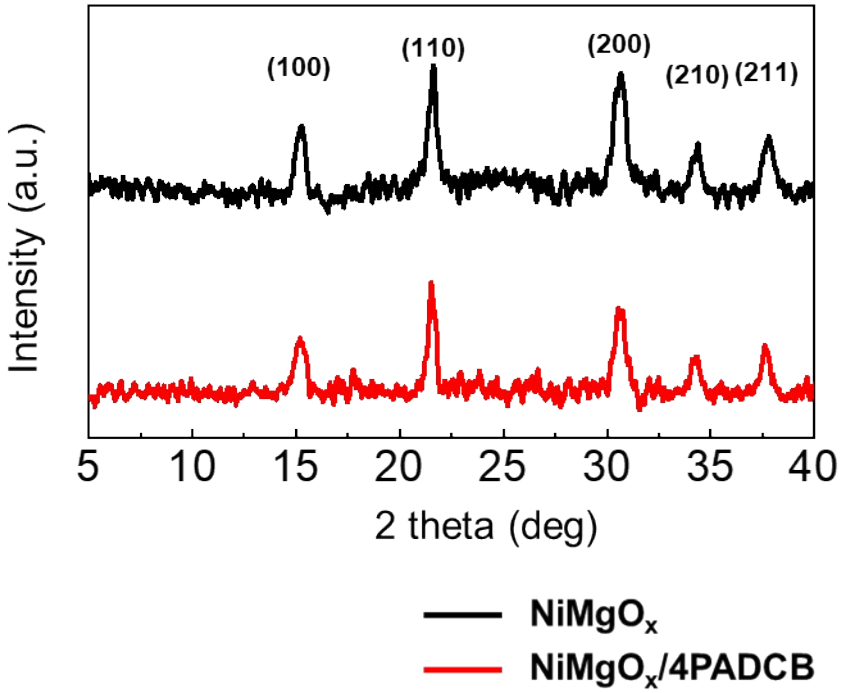

Figure S7. XRD spectra of perovskite on $NiMgO_x$ and $NiMgO_x$/4PADCB layers.

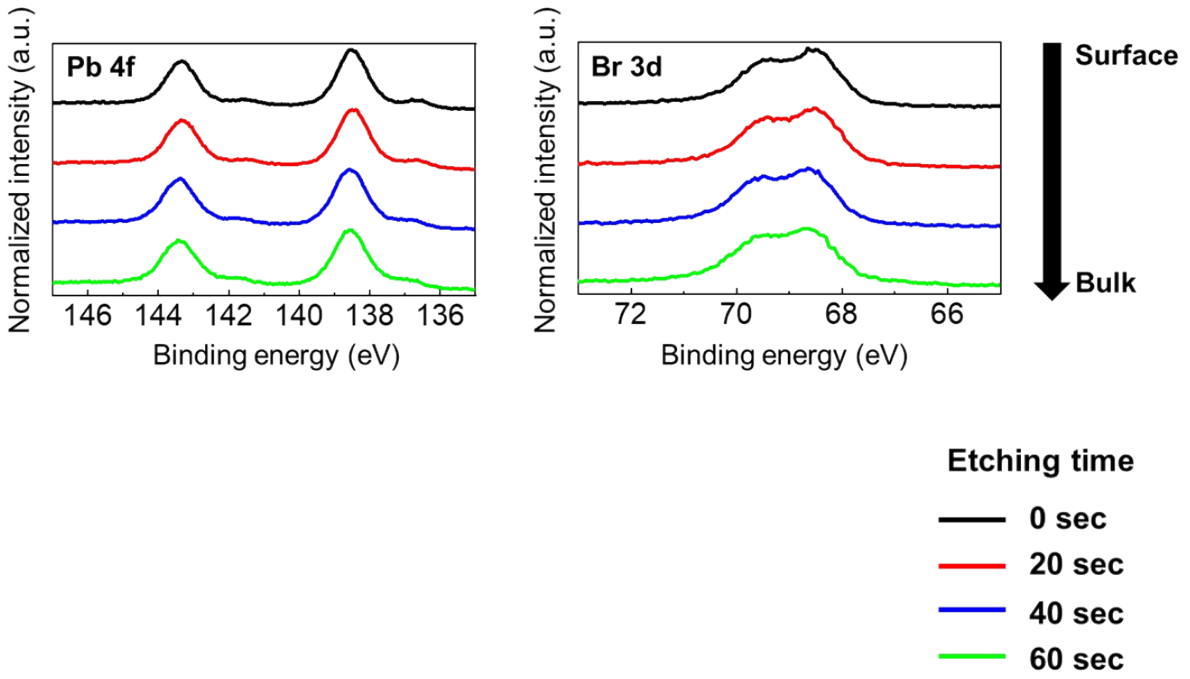

Figure S8. XPS depth profile analysis showing the evolution of the Pb 4f and Br 3d core-level spectra with etching time on $NiMgO_x$/4PADCB surface.

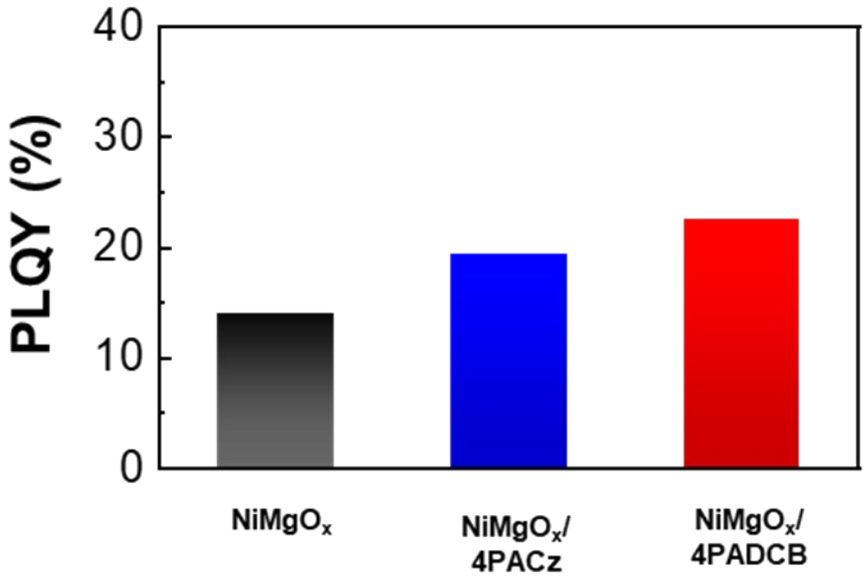

Figure S9. Photoluminescence quantum yield (PLQY) of perovskite on $NiMgO_x$ with and without SAM interlayers.

78

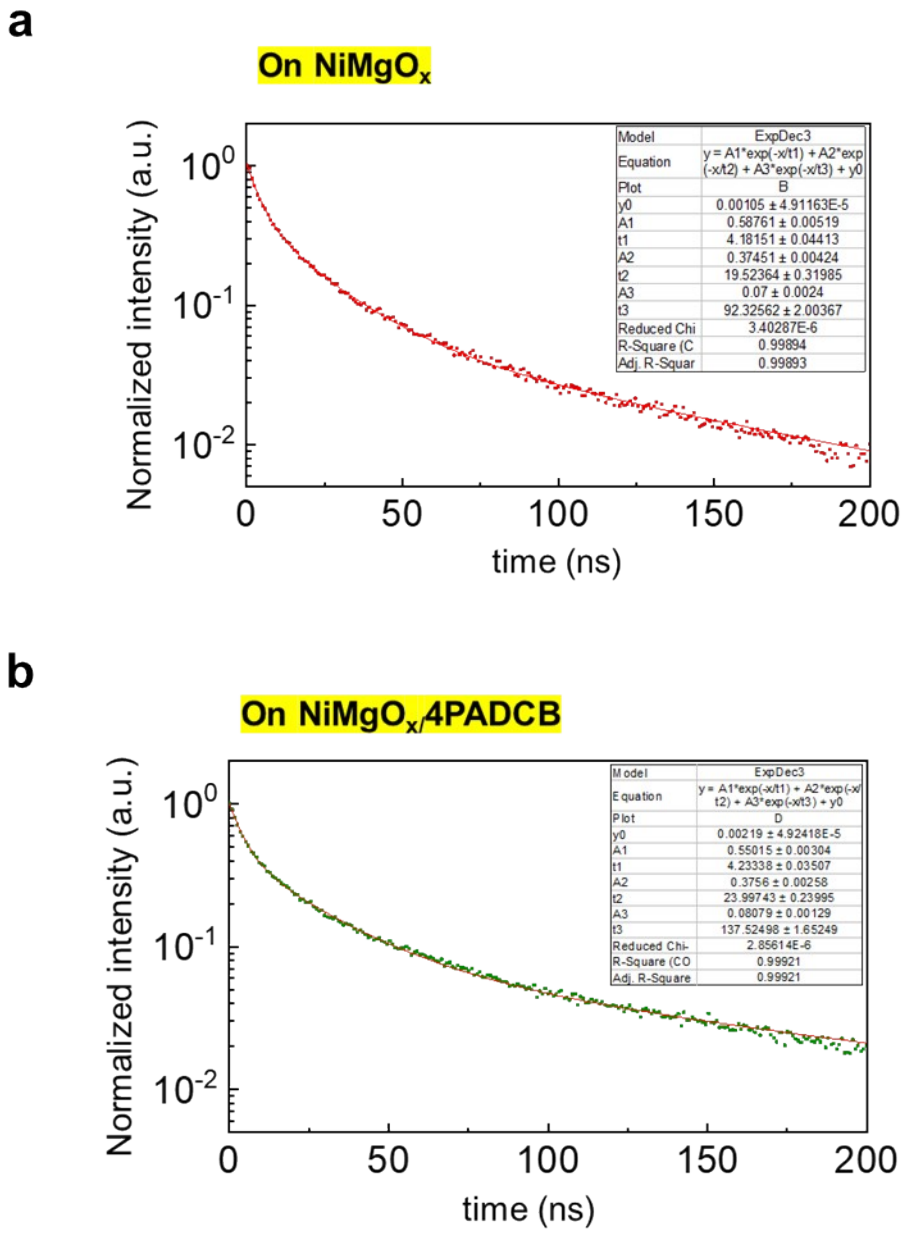

79

80

81 **Figure S10.** TrPL fitting data using a tri-exponential decay method. The fitting sample is
82 perovskite on (a) $NiMgO_x$, and (b) $NiMgO_x$/4PADCB layers.

83

84

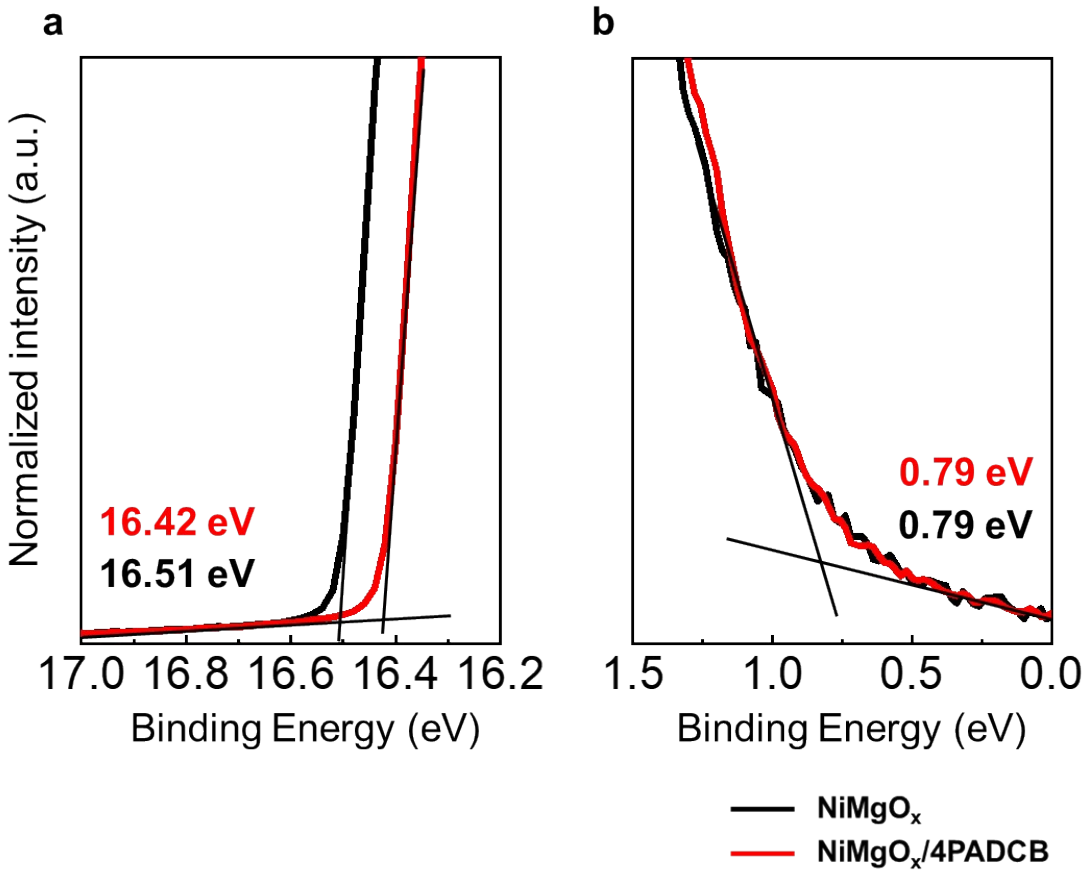

Figure S11. UPS spectra of perovskite on $NiMgO_x$ and $NiMgO_x$/4PADCB layers. (a) Secondary cut-off and (b) edge regions of spectra.

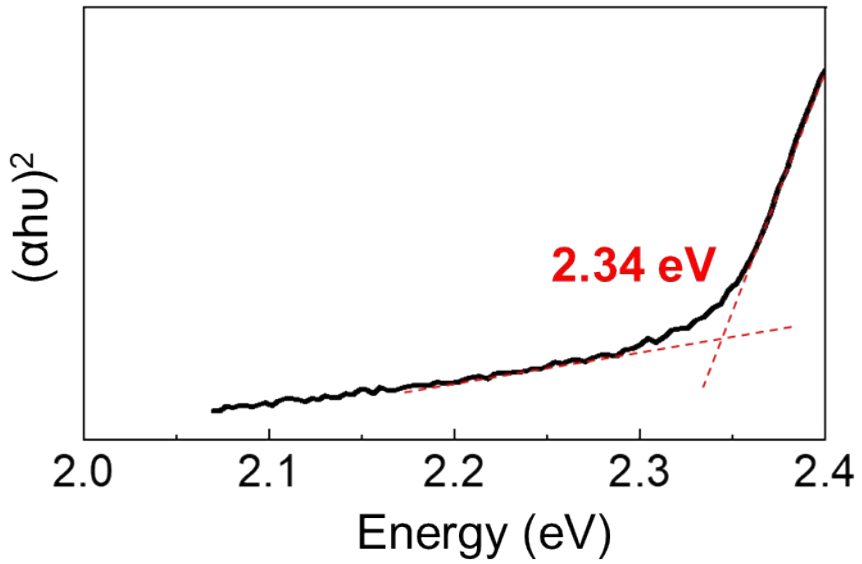

Figure S12. Tauc plot of the perovskite layers, showing an optical bandgap of 2.34 eV, consistent with the green emission region.

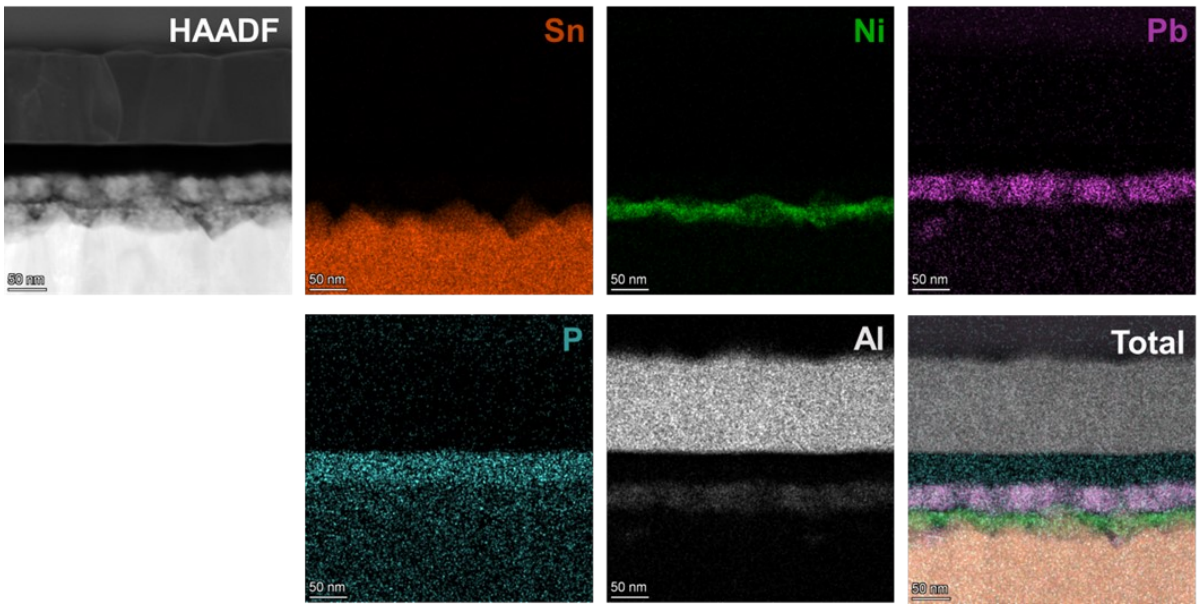

Figure S13. High-angle annular dark-field (HAADF) image and EDS spectra of the PeLED. Each layer is successfully deposited, as evidenced by the distinct elemental distributions.

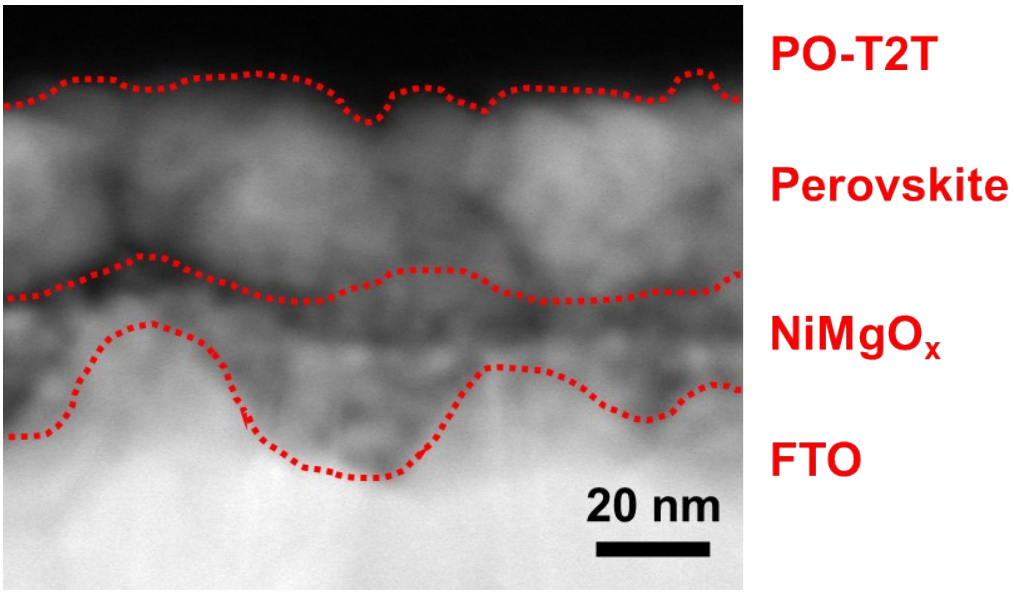

Figure S14. High-magnification cross-sectional STEM image of the PeLED, showing clearly distinguishable layers.

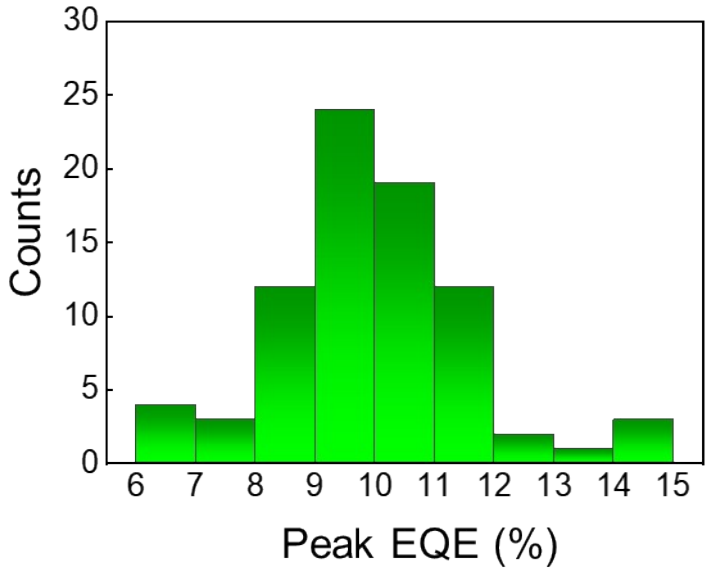

Figure S15. Histogram of peak EQE for 80 devices with the 4PADCB interlayer (FTO/NiMgO$_x$/4PADCB/perovskite/PO-T2T/LiF/Al). The average EQE is 10.0%.

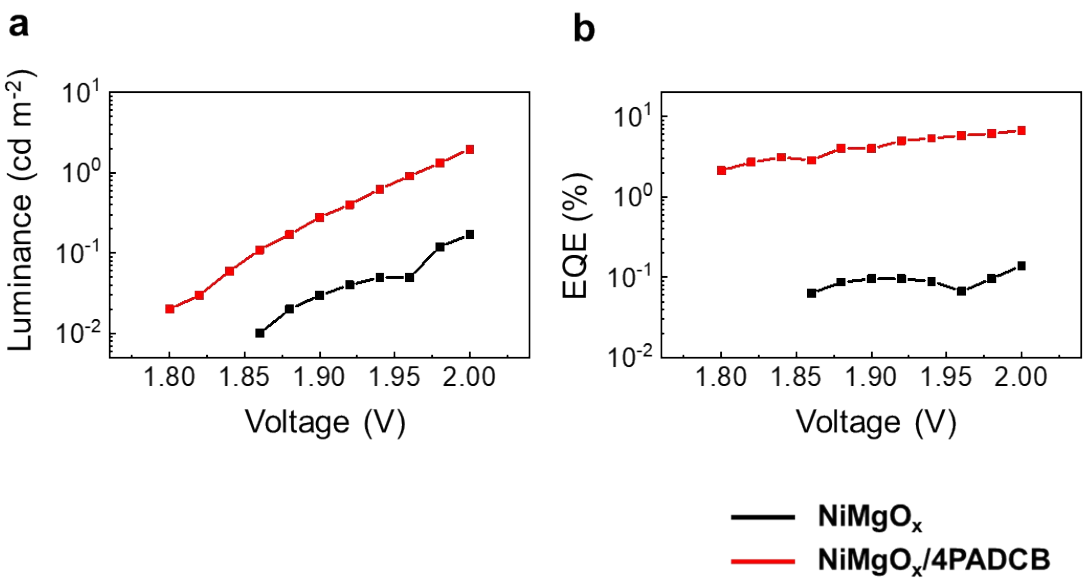

Figure S16. (a) Luminance and (b) EQE relationship at low operating voltage (~ 2 V) w/ and w/o 4PADCB interlayers.

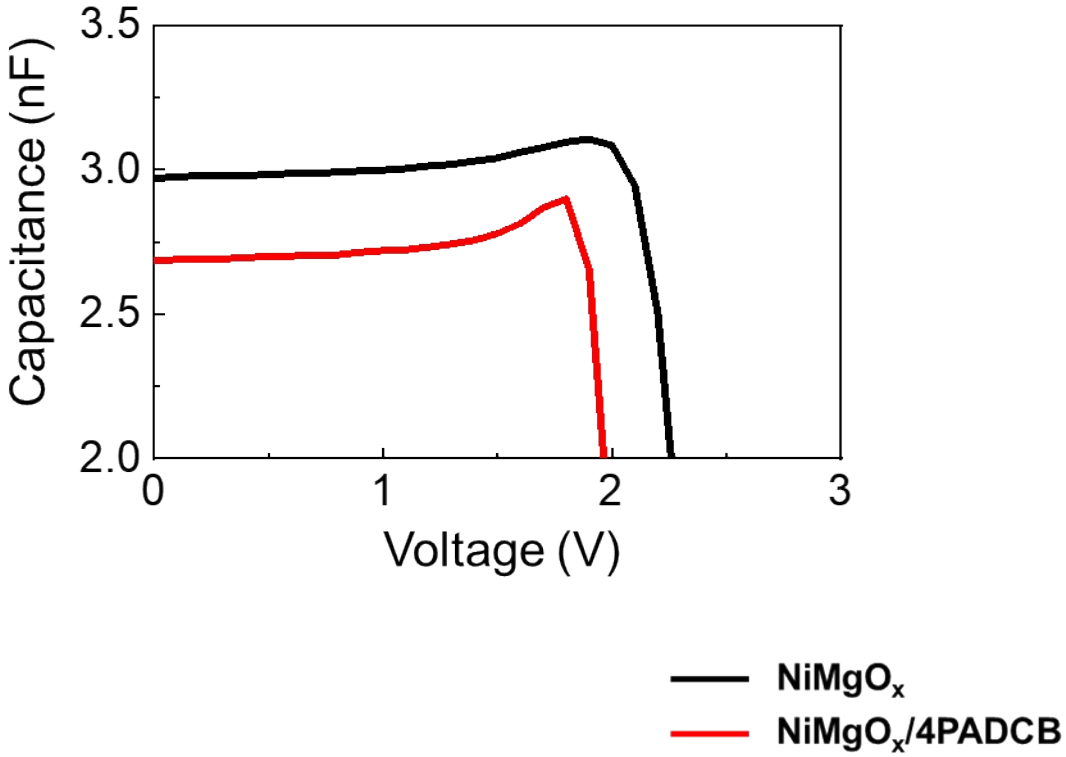

Figure S17. The capacitance-voltage (C-V) relationship of PeLED w/ and w/o 4PADCB interlayers.

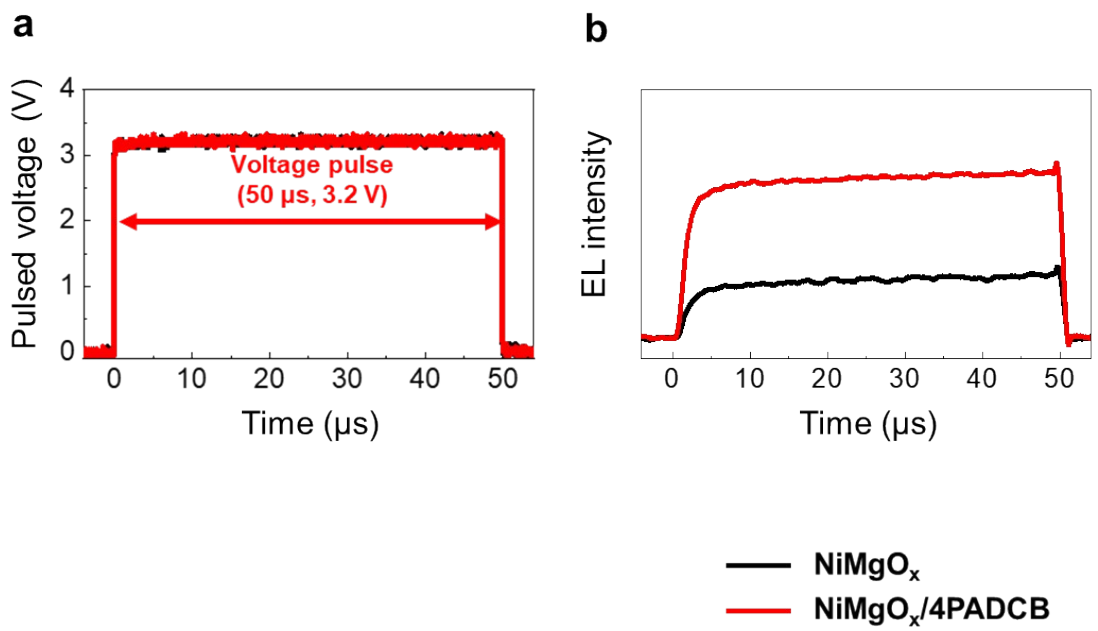

Figure S18. Pulsed voltage and time relationship during TrEL measurements. (a) the pulsed voltage was 3.2 V with 50 μs periods and (b) absolute transient EL (TrEL) spectra w/ and w/o the 4PADCB interlayer.

144

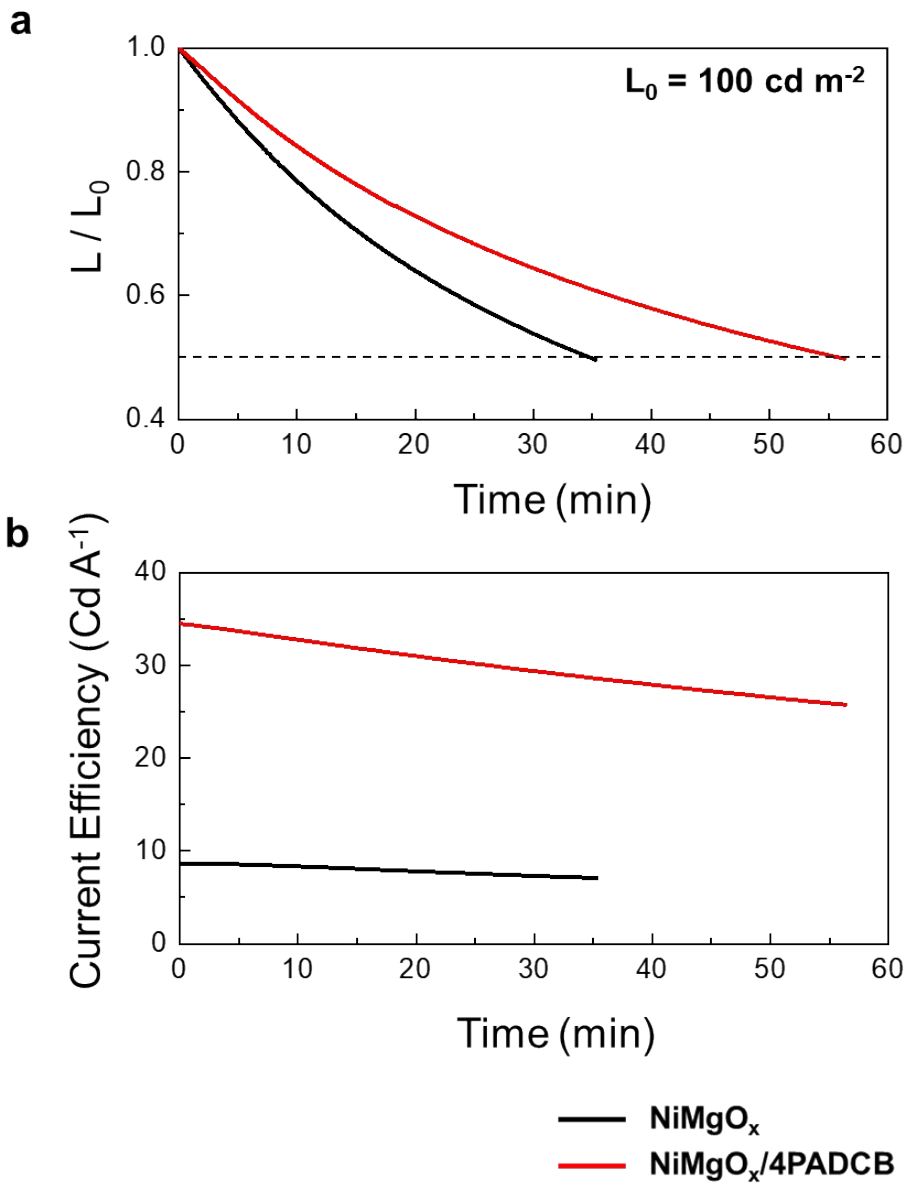

145

146

147 **Figure S19.** Device stability test with time variation. The results indicate (a) luminance-time
148 (L-t) relationship and (b) current efficiency-time (CE-t) relationship.
149

150

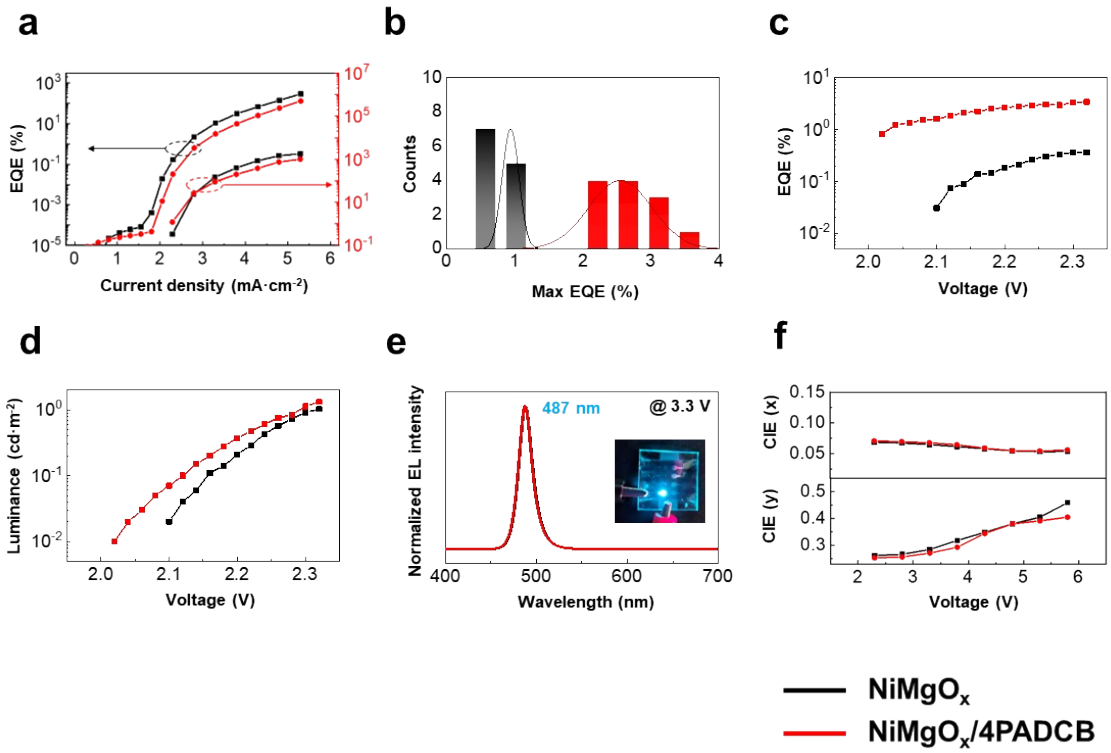

Figure S20. Sky-blue PeLED characterization w/ and w/o 4PADCB interlayer molecules. (a) J-V-L characteristics and (b) derivation of maximum EQE. (c) EQE and (d) luminance curves in the sub-bandgap voltage region (~2.3 V) for each device. (e) Normalized electroluminescence (EL) spectra at a 3.3 V bias and demonstration image of sky-blue PeLEDs with and without 4PADCB interlayers. (f) Color stability evaluated by CIE coordinate shift under bias.

	λ_{PL} (nm)	A_1	τ_1 (ns)	A_2	τ_2 (ns)	A_3	τ_3 (ns)	τ_{avg} (ns)	R^2
On $Ni_{0.9}Mg_{0.1}O_x$	521	0.587	4.18	0.374	19.52	0.07	92.32	46.2	0.999
On $Ni_{0.9}Mg_{0.1}O_x$/4PADCB	521	0.550	4.23	0.375	23.99	0.081	137.5	77.9	0.999

Table S1. Fitting parameter summary of TrPL curves. TrPL fitting was performed using tri-exponential decay curve which composed fast-decay (A_1, τ_1), moderate-decay (A_2, τ_2) and slow-decay (A_3, τ_3). The fast-decay component is related to non-radiative recombination by trap state, whereas moderate and slow decay are related to radiative recombination, respectively. The average PL lifetime (τ_{avg}) is calculated from formula $\tau_{avg} = \frac{A_1\tau_1^2 + A_2\tau_2^2 + A_3\tau_3^2}{A_1\tau_1 + A_2\tau_2 + A_3\tau_3}$.

173

	λ_{EL} (nm)	V_{on} at 1 cd m^{-2} (V)	L_{max} (cd m^{-2}) (at bias (V))	EQE_{max} (%) (at bias (V))	CE_{max} (cd A^{-1}) (at bias (V))	PE_{max} (lm W^{-1}) (at bias (V))
$Ni_{0.9}Mg_{0.1}O_x$	521	2.12	22,634 (4.8)	5.51 (3.8)	20.51 (3.8)	16.96 (3.8)
$Ni_{0.9}Mg_{0.1}O_x$/4PACz	521	2.06	29,822 (4.8)	6.76 (3.8)	24.99 (3.8)	20.88 (3.3)
$Ni_{0.9}Mg_{0.1}O_x$/4PADCB	521	1.96	38,557 (5.3)	14.38 (3.3)	53.61 (3.3)	59.81 (2.8)
$Ni_{0.9}Mg_{0.1}O_x$	487	2.32	1,748 (5.3)	1.07 (3.3)	1.38 (3.3)	1.31 (3.3)
$Ni_{0.9}Mg_{0.1}O_x$/4PADCB	487	2.29	1,049 (5.3)	3.31 (2.8)	4.00 (2.8)	4.94 (2.3)

174

175

176 **Table S2.** Summarized PeLED characteristics with and without SAM interlayers on $NiMgO_x$.